**AALBORG UNIVERSITY**

# Improved DC-Link Voltage Regulation Strategy for Grid-Connected Converters

Gui, Yonghao; Blaabjerg, Frede; Wang, Xiongfei; Bendtsen, Jan Dimon; Yang, Dongsheng; Stoustrup, Jakob

*Publication date:*
2021

*Document Version*
Accepted author manuscript, peer reviewed version

[Link to publication from Aalborg University](Link to publication from Aalborg University)

# Improved DC-Link Voltage Regulation Strategy for Grid-Connected Converters

Yonghao Gui, *Member, IEEE*, Frede Blaabjerg, *Fellow, IEEE*, Xiongfei Wang, *Senior Member, IEEE*, Jan D. Bendtsen, *Member, IEEE*, Dongsheng Yang, *Senior Member, IEEE*, and Jakob Stoustrup, *Senior Member, IEEE*.

*Abstract*—In this paper, an improved dc-link voltage regulation strategy is proposed for grid-connected converters applied in dc microgrids. For the inner loop of the grid-connected converter, a voltage modulated direct power control is employed to obtain two second-order linear time-invariant systems, which guarantees that the closed-loop system is globally exponentially stable. For the outer loop, a sliding mode control strategy with a load current sensor is employed to maintain a constant dc-link voltage even in the presence of constant power loads at the dc-side, which adversely affect the system stability. Furthermore, an observer for the dc-link current is designed to remove the dc current sensor at the same time improving the reliability and decreasing the cost. From both simulation and experimental results obtained from a 15-kVA prototype setup, the proposed method is demonstrated to improve the transient performance of the system and has robustness properties to handle parameter mismatches compared with the input-output linearization method.

*Index Terms*—Dc microgrid, direct power control, grid-connected converter, observer, sliding mode control.

## I. INTRODUCTION

**T**HREE-phase ac/dc power converters (rectifiers), which convert the ac power to dc using pulse-width modulation (PWM), are widely used in various applications, e.g., dc microgrids [1], renewable energy sources [2], uninterruptible power supplies [3], etc. Maintaining the dc-link voltage at a certain constant level is one of the key control objectives of such rectifier systems.

Generally, the control strategies of PWM rectifier systems consists of two parts, denoted inner-loop and outer-loop [4]. Conventionally, vector current control (VCC) is used for the inner loop where two decoupled *d-q* axes current controllers are designed in a synchronous rotating reference frame [5]. This control strategy has the advantage that the relevant signals are transformed from ac to dc, *i.e.*, the tracking problem is

changed into a regulation problem. However, a phase locked loop (PLL), which estimates the phase of the grid voltage for the Park transformation, suffers from a slow dynamical response when the initial conditions are different from the measurements.

To overcome such issues, a direct power control (DPC) scheme is designed through the calculation of active and reactive power signals [6], eliminating the need for inner-loop current regulators. However, due to a variable switching frequency, it is not easy to design an output filter. To overcome this problem, the space vector PWM based DPC method has been proposed, which achieves a constant switching frequency [7], [8]. Based on that strategy, various techniques have been employed for control, *e.g.*, sliding-mode control (SMC) [9], passivity-based control [10], and model predictive control [11], etc. However, the steady-state performance is still worse than by using the VCC methods. Recently, the relationship between a DPC model and a system model in the *d-q* frame has been investigated [12], where the DPC method obtains the same steady-state performance as VCC without compromising the transient performance. In [13], it is shown that the voltage modulated (VM)-DPC improves the performance compared with the SMC and PBC. For that reason, this concept has been employed in various applications under different conditions [14]–[20]. Consequently, the VM-DPC method is applied to the inner loop of the rectifier system in this paper.

For the outer loop (dc-link voltage controller), the main objective is to regulate the dc-link voltage to a constant value. Conventionally, a proportional-integral (PI) controller is used in the outer loop controller, where a *d*-axis current or real power reference for the inner loop is generated [21]. However, the performance will be affected by the load disturbances connected in dc microgrids. To handle this problem, feedforward control techniques have been studied by considering the mismatched power/current disturbances in order to obtain an enhanced dynamic performance of the dc-link voltage [22]–[25]. However, they will be affected by the different operating points since the controller gains are tuned at a certain operating point. An adaptive PI controller is proposed to improve the dc-voltage performance at different operating points [26]. However, it does not consider the nonlinearity in the dc-link voltage dynamics. In order to obtain a fast performance in the whole operating range, nonlinear control strategies have been proposed. Input-output linearization (IOL) methods were employed to cancel the nonlinear characteristics of the

system dynamics in [27], [28]. However, they are sensitive to parameter uncertainties. In order to improve the robustness, super-twisting algorithm based SMC and backstepping control methods have been designed for rectifier systems [14], [29]. However, they are using a load current sensor to cancel the nonlinearity or reject the influence of it. In addition, to remove the load current sensor at the dc-link for the improvement of the reliability and decrease the cost, dc-link current observers are designed to identify the load current or power disturbance [30]–[32]. Recently, an extended state observer is proposed to reject the load connected at the dc-side [29]. However, it is not easy for the tuning and also the nonlinear analysis.

In summary, the current state-of-the-art is to apply the aforementioned methods for VCC or robust controller in the synchronous rotating reference frame for the inner-loop and some advanced control strategies for the outer-loop. The key component, the PLL, in such methods will cause a slow transient response or even stability problems in a weak grid as discussed in [33]. Other methods are to use the DPC for the inner-loop and some advanced control strategies for the outer-loop. Although, the DPC obtains faster transient response, the steady-state performance becomes worse compared with the VCC. It should be noted that the inner-loop (VM-DPC) was recently designed for the grid-connected inverter, and it combines advantages of DPC and VCC, e.g., fast transient response due to the elimination of PLL, better steady-state performance at the same level as the VCC, simple yet robust property, etc. [12]. This is the motivation to use the VM-DPC in the inner-loop. Moreover, the outer-loop was designed to cancel the nonlinear terms with the consideration of the dc-link voltage dynamics as discussed in [26], which is compared to the proposed method.

The main contributions can be summarized as follows:

1) A simple yet robust nonlinear controller: We firstly design the SMC with the modified VM-DPC for the rectifier system. The VM-DPC is employed into the inner-loop control in order to obtain both advantages of DPC and VCC, e.g., fast transient response due to the elimination of PLL and good steady-state performance at the same level as the VCC, etc. In addition, it is simple and robust. For the outer-loop, since the dc-link voltage dynamics is nonlinear, an SMC is employed to regulate the dc-link voltage in order to utilize its advantages, e.g., robust to external disturbances, high accuracy, and finite time convergence, etc. [34].

2) Improvement of the reliability and decrease the cost: A dc-link current observer is designed to improve the reliability and decrease the cost of the system instead of using a measurement. In addition, the observer can reduce harmonic oscillations at the dc-side caused by the unbalanced ac currents.

3) Experimental test: The experimental results obtained with the proposed method are in excellent agreement with the simulation results obtained from MAT-LAB/Simulink and PLECS. These results provide support for the practical feasibility of the proposed method. Compared with the IOL method, an enhanced transient
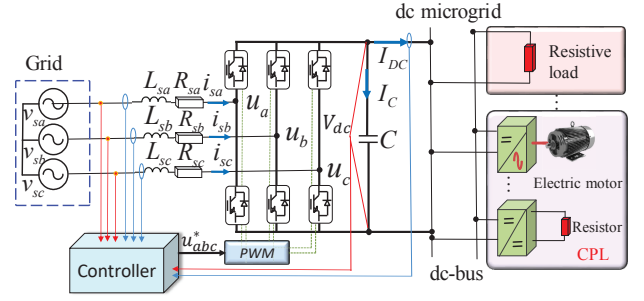


Fig. 1. Rectifier system in dc microgrid. (CPL: Constant Power Load)

performance and robustness to parameter mismatches are obtained. In addition, compared with the SMC using the measurement, the transient response is slightly worsened but the steady-state performance is improved.

Although the SMC with the VM-DPC algorithm was initially designed for the three-phase rectifier system in [35], issues related to removal of current sensor, implementation of strategies, and experimental verification have not yet been addressed. This paper makes an important contribution to the practical concerns by addressing these issues. Consequently, based on this paper, the users have two options of rectifier control: one is to prioritize the transient response with the SMC using measurement, e.g., smaller overshoot, faster convergence time, more robustness properties, etc. The other one is to prioritize the steady-state performance with the SMC using the dc-link current observer, e.g., less harmonic oscillations on the dc-side, reduction of cost, improvement of reliability of the dc capacitor, etc. In addition, various grid voltage estimation methods have been researched in order to reduce the number of grid voltage sensors and improve the reliability of the system [36]–[40].. This is considered out of scope of the current paper, but will be a subject of future research.

## II. MODELING OF PWM RECTIFIER SYSTEM

In this section, we will briefly introduce the PWM rectifier system model. A typical three-phase two-level PWM rectifier connected to the grid with an L-filter is shown in Fig. 1. It can be observed that one of the objectives of the PWM rectifier is to support power into the dc microgrid. Normally, the three-phase grid voltages, $v_{s,abc}$, the line current, $i_{s,abc}$, the voltage at the dc-link, $V_{dc}$, and the dc current flowing into the load, $I_{dc}$, are measured to generate the rectifier voltages, $u_{abc}$, which are used to control the PWM rectifier. $L_{s,abc}$ and $R_{s,abc}$ are filter inductance and resistance, respectively. In addition, different types of loads are connected to the dc microgrid. One is a linear load (*e.g.*, resistor), the other is a CPL (*e.g.*, power converter and motor, etc.), as shown in Fig. 1.

### A. Model of Ac-Side of Rectifier

In this paper, the relationship between the grid voltage and converter voltage could be described with the consideration of a balanced grid voltage as follows [41]:

$$v_{s,abc} = R_{s,abc} i_{s,abc} + L_{s,abc} \frac{di_{s,abc}}{dt} + u_{abc}, \qquad (1)$$

**Assumption 1.** *It is assumed that the filter resistances and inductances are the same in each phase.*

The dynamics in (1) can be transformed into the stationary reference frame through Clark transformation as

$$v_{s\alpha} = R_s i_{s\alpha} + L_s \frac{di_{s\alpha}}{dt} + u_\alpha,$$
$$v_{s\beta} = R_s i_{s\beta} + L_s \frac{di_{s\beta}}{dt} + u_\beta, \tag{2}$$

where $v_{s\alpha,\beta}$, $i_{s\alpha,\beta}$, and $u_{\alpha,\beta}$ indicate the grid voltage, output currents, and the rectifier voltages in the stationary reference frame, respectively.

The instantaneous real and reactive power signals can be defined as

$$P = \frac{3}{2}(v_{s\alpha}i_{s\alpha} + v_{s\beta}i_{s\beta}),$$
$$Q = \frac{3}{2}(v_{s\beta}i_{s\alpha} - v_{s\alpha}i_{s\beta}), \tag{3}$$

where $P$ and $Q$ are the real and reactive powers at ac-side. If we differentiate the injected active and reactive powers of rectifier system in (3) with respect to time, then their variations can be expressed as

$$\frac{dP}{dt} = \frac{3}{2}\left( i_{s\alpha}\frac{dv_{s\alpha}}{dt} + v_{s\alpha}\frac{di_{s\alpha}}{dt} + i_{s\beta}\frac{dv_{s\beta}}{dt} + v_{s\beta}\frac{di_{s\beta}}{dt} \right),$$
$$\frac{dQ}{dt} = \frac{3}{2}\left( i_{s\alpha}\frac{dv_{s\beta}}{dt} + v_{s\beta}\frac{di_{s\alpha}}{dt} - i_{s\beta}\frac{dv_{s\alpha}}{dt} - v_{s\alpha}\frac{di_{s\beta}}{dt} \right). \tag{4}$$

**Assumption 2.** *It is assumed that the grid voltages in the stationary reference frame are represented as*

$$v_{s\alpha} = V_s\cos(\omega t),$$
$$v_{s\beta} = V_s\sin(\omega t), \tag{5}$$

*where $V_s$ and $\omega$ are the magnitude and angular frequency of grid voltage, respectively.*

Assumption 2 is reasonable since a non-distorted grid is considered in the paper. The derivative of the grid voltage in (5) with respect to time can be expressed as

$$\frac{dv_{s\alpha}}{dt} = -\omega V_s\sin(\omega t) = -\omega v_{s\beta},$$
$$\frac{dv_{s\beta}}{dt} = \omega V_s\cos(\omega t) = \omega v_{s\alpha}. \tag{6}$$

Considering (2) to (6), the dynamics of the ac-side with respect to the real and reactive powers can be expressed as

$$\frac{dP}{dt} = -\frac{R_s}{L_s}P - \omega Q + \frac{3}{2L_s}(v_{s\alpha}u_\alpha + v_{s\beta}u_\beta) - \frac{3}{2L_s}V_s^2,$$
$$\frac{dQ}{dt} = \omega P - \frac{R_s}{L}Q + \frac{3}{2L_s}(v_{s\beta}u_\alpha - v_{s\alpha}u_\beta). \tag{7}$$

where $u_\alpha$ and $u_\beta$ are the control inputs (rectifier voltages).

**Remark 1.** *Notice that the dynamics of the injected real and reactive powers in (7) describe a time-varying system since the grid voltages are multiplied by the control inputs.*
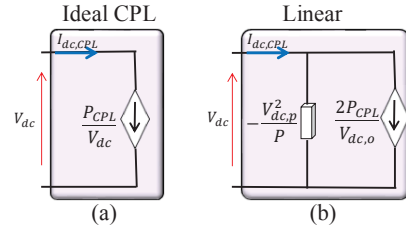


Fig. 2. Equivalent CPL Model. (a) Ideal CPL; (b) Linearized CPL.

### B. Model of Dc-Side of Rectifier

At first, the system losses are neglected to model the dc-side. Thus, the dynamics at the dc-side can be expressed with the power variation in the dc-link capacitor as

$$CV_{dc}\frac{dV_{dc}}{dt} = P_{cap} = P_{rec} - P_{load}, \tag{8}$$

where $P_{cap}$ indicates the real power stored in the capacitor at the dc-side, $P_{rec}$ indicates the injected real power of the rectifier system from ac to dc-side, and $P_{load}$ is the consumed power by the load connected to the dc-side. It can be formulated as follows:

$$P_{load} = V_{dc}I_{dc}. \tag{9}$$

Consequently, the dynamics of the dc-link voltage could be simplified by substituting (9) into (8) such as

$$\frac{dV_{dc}}{dt} = \frac{P_{rec}}{C}\frac{1}{V_{dc}} - \frac{1}{C}I_{dc}. \tag{10}$$

**Remark 2.** *Notice that the dc-link voltage dynamics in (10) is a nonlinear system since the dc-link voltage is in the denominator.*

### C. Model of Load at Dc-Link

First, the output current, $I_{dc}$, consists of the currents of the resistive load and CPL.

$$I_{dc} = I_{dc,R} + I_{dc,CPL}(v), \tag{11}$$

where $I_{dc,R}$ and $I_{dc,CPL}$ indicate the dc-link output currents for resistive load and the CPL, respectively. The resistive load is considered as

$$I_{dc,R} = C_R V_{dc}, \tag{12}$$

where $C_R$ represents the conductance of the resistive load. Further, an ideal CPL model is nonlinear; thus, it is common practice to linearize it at a dc-link voltage operating point, $V_{dc,o}$, shown as [42]

$$I_{dc,CPL}(v) \approx 2\frac{P_{CPL}}{V_{dc,o}} + \frac{v}{\frac{-P_{CPL}}{V_{dc,o}^2}}, \tag{13}$$

where $P_{CPL}$ is the constant power. It should be noted that $v = V_{dc}$ in (13) and $V_{op}$ is an operating point value (steady-state value). In (13), the first term is similar to a constant current load and the second term is the negative resistance part. Each CPL is connected to the dc microgrid through a transmission line, as depicted in the equivalent model shown in Fig. 2.

### III. CONTROLLER DESIGN FOR PWM RECTIFIER

There are various controllers, which are designed based on the dynamics in (7) directly [9], [10]. However, the steady-state performances in terms of real and reactive powers are not good since the dynamics in (7) is a time-varying system. Recently, a relationship between the DPC model and system model in the $d$-$q$ frame is investigated [12]. One of the most important merits is that it obtains a linear time invariant system for the DPC model.

#### A. Voltage Modulated DPC

The new VM inputs are set as follows [43]:

$$u_{GVM1} = v_{s\alpha}u_{\alpha} + v_{s\beta}u_{\beta},$$
$$u_{GVM1} = v_{s\beta}u_{\alpha} - v_{s\alpha}u_{\beta} \tag{14}$$

**Remark 3.** *With the new control inputs defined in* (14) *the dynamics of the active and reactive powers of the rectifier in* (7) *are changed into an LTI system as*

$$\frac{dP}{dt} = -\frac{R_s}{L_s}P - \omega Q - \frac{3}{2L_s}V_s^2 + \frac{3}{2L_s}u_{GVM1},$$
$$\frac{dQ}{dt} = \omega P - \frac{R_s}{L_s}Q + \frac{3}{2L_s}u_{GVM2}. \tag{15}$$

**Definition 1.** *The errors of injected active and reactive powers of the rectifier are defined as*

$$e_P := P^* - P,$$
$$e_Q := Q^* - Q, \tag{16}$$

*where $P^*$ and $Q^*$ are the injected active and reactive power references at the ac-side, respectively.*

**Theorem 1.** *Consider the system in* (15) *and the controller*

$$u_{GVM1}. = \frac{2L_s}{3}\left(\frac{R_s}{L_s}P + \omega Q + \frac{3}{2L_s}V_s^2 + K_{Pp}e_P + K_{Pi}\int e_P dt\right),$$
$$u_{GVM2}. = \frac{2L_s}{3}\left(-\omega P + \frac{R_s}{L_s}Q + K_{Qp}e_Q + K_{Qi}\int e_Q dt\right), \tag{17}$$

*where $K_{Pp}$, $K_{Pi}$, $K_{Qp}$, and $K_{Qi}$ are any positive values; the closed-loop interconnection of the system and controller is exponentially stable.* ◇

*Proof.* At the first step, the error dynamics are obtained as

$$\dot{e}_P = \dot{P}^* - \dot{P},$$
$$\dot{e}_Q = \dot{Q}^* - \dot{Q}. \tag{18}$$

For the sake of simplicity, $P^*$ and $Q^*$ are considered as constants in this part. Then, (18) is changed to

$$\dot{e}_P = \frac{R_s}{L_s}P + \omega Q + \frac{3}{2L_s}V_s^2 - \frac{3}{2L_s}u_{GVM1},$$
$$\dot{e}_Q = -\omega P + \frac{R_s}{L_s}Q - \frac{3}{2L_s}u_{GVM2}. \tag{19}$$

If substituting (17) into (19), the closed-loop system can be obtained as

$$\dot{e}_P = -K_{Pp}e_P - K_{Oi}\int e_P dt,$$
$$\dot{e}_Q = -K_{Qp}e_Q - K_{Qi}\int e_Q dt. \tag{20}$$

If the following variables are defined as

$$\psi_P = e_P, \quad \psi_Q = e_Q, \tag{21}$$

then, the whole closed-loop system can be expressed with the combination of (20) and (21) like:

$$\underbrace{\begin{bmatrix} \dot{e}_P \\ \dot{\psi}_P \\ \dot{e}_Q \\ \dot{\psi}_Q \end{bmatrix}}_{\dot{x}} = \underbrace{\begin{bmatrix} -K_{Pp} & -K_{Pi} & 0 & 0 \\ 1 & 0 & 0 & 0 \\ 0 & 0 & -K_{Qp} & -K_{Qi} \\ 0 & 0 & 1 & 0 \end{bmatrix}}_{A_c} \underbrace{\begin{bmatrix} e_P \\ \psi_P \\ e_Q \\ \psi_Q \end{bmatrix}}_{x}. \tag{22}$$

It should be noted that $x$ and $A_c$ are the state and the state-space matrix of the closed-loop system in (22), respectively. It is obvious that if $K_{Pp} > 0$, $K_{Pi} > 0$, $K_{Qp} > 0$, and $K_{Qi} > 0$, then all the eigenvalues of $A_c$ have negative real part, i.e., the closed-loop system is exponentially stable. □

Finally, the original control inputs are obtained as

$$u_{\alpha} = \frac{v_{s\alpha}u_{GVM1} - v_{s\beta}u_{GVM2}}{V_s^2}, \quad u_{\beta} = \frac{v_{s\beta}u_{GVM1} + v_{s\alpha}u_{GVM2}}{V_s^2}. \tag{23}$$

#### B. Dc-Link Voltage Controller

In this part, the main objective is to control the dc-link voltage at a constant level even in the presence of uncertainties or disturbances. For this reason, an SMC method is designed to obtain an enhanced performance in terms of the dc-link voltage.

**Definition 2.** *The error of the dc-link voltage is defined as follows:*

$$e_{V_{dc}} = V_{dc}^* - V_{dc}, \tag{24}$$

*where $V_{dc}^*$ is the reference of $V_{dc}$.*

**Definition 3.** *A sliding surface, s, is defined as*

$$s = K_{P,V_{dc}}e_{V_{dc}} + K_{I,V_{dc}}\int e_{V_{dc}}dt, \tag{25}$$

*where $K_{P,V_{dc}}$ and $K_{I,V_{dc}}$ are the controller gains. $V_{dc}^*$ is reference of $V_{dc}$.*

Then, on the sliding surface (i.e., $s = 0$), the motion is governed by

$$K_{P,V_{dc}}e_{V_{dc}} + K_{I,V_{dc}}\int e_{V_{dc}}dt = 0. \tag{26}$$

It can be seen that choosing $K_{P,V_{dc}} > 0$ and $K_{I,V_{dc}} > 0$ guarantees that $V_{dc}$ converges to $V_{dc}^*$ as $t \to \infty$. In addition, the convergence rate can be determined through $K_{P,V_{dc}}$ and $K_{I,V_{dc}}$. Moreover, in the SMC method, the following equation is also satisfied.

$$\dot{s} = K_{P,V_{dc}}(\dot{V}_{dc}^* - \dot{V}_{dc}) + K_{I,V_{dc}}e_{V_{dc}}. \tag{27}$$

**Theorem 2.** *Consider the system in* (10)*, if a control law is taken as follows:*

$$P_{rec} = I_{dc}V_{dc} + \frac{K_{I,V_{dc}}CV_{dc}}{K_{P,V_{dc}}}e_{V_{dc}} + K_s\text{sat}(\frac{s}{\varepsilon}), \tag{28}$$
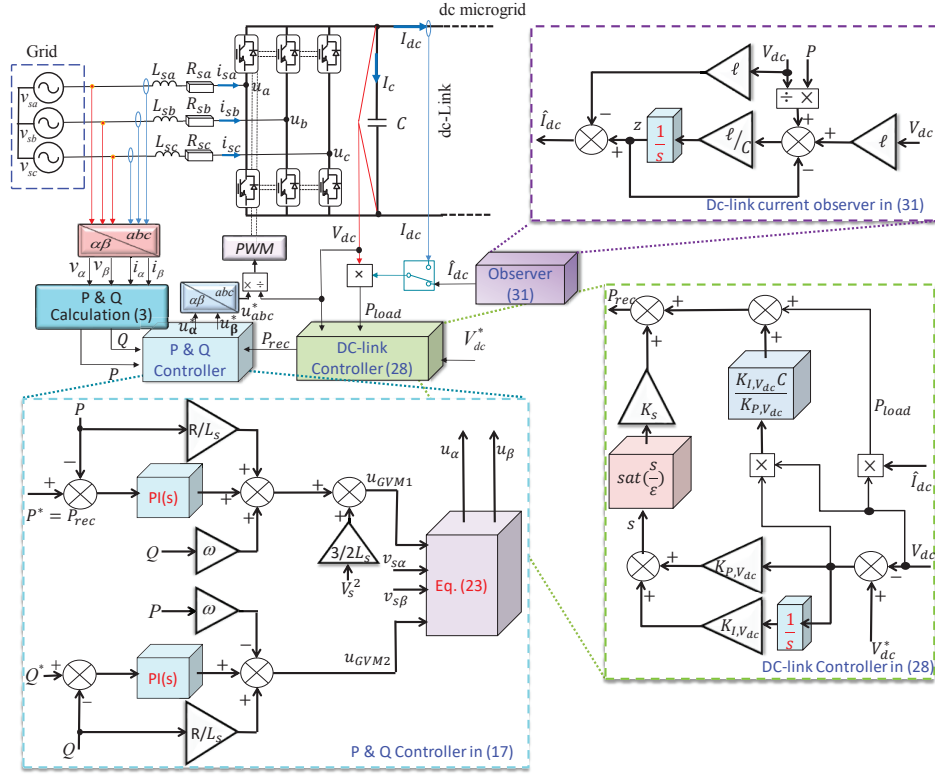
Fig. 3. Block diagram of the proposed control method (SMC with observer) for a rectifier system in the dc microgrid.

*where*

$$\text{sat}(\frac{s}{\varepsilon}) = \begin{cases} \dfrac{s}{\varepsilon}, & \text{if } |s| \le |\varepsilon| \\ +1, & \text{if } s > \varepsilon \\ -1, & \text{if } s < -\varepsilon \end{cases},$$

*and $\varepsilon$ is a positive constant value and taking the controller gain $K_s > 0$, then the system trajectory reaches the boundary layer $|s| \le \varepsilon$ in finite time.*

We omitted the proof of Theorem 2; it can be found in [35].

**Remark 4.** *In order to remove the chattering phenomenon, a saturation function is used instead of the signum function.*

**Remark 5.** *From Theorem 2, it can be concluded that $V_{dc}$ reaches the boundary layer $|s| \le \varepsilon$ in finite time. After that, $V_{dc}$ converges to $V_{dc}^*$ as $t \to \infty$ based on (26).*

Even when there exists a CPL in the dc microgrid, the conditions of Theorem 2 are satisfied, i.e., $V_{dc}$ reaches the boundary layer $|s| \le \varepsilon$ in finite time.

**Remark 6.** *The generated control input, $P_{rec}$ in (28), is sent to the reference of the real power in (17).*

### C. Dc-Link Current Observer

In this part, an observer of the dc-link current is designed to remove the current sensor.

**Assumption 3.** *The dc-link current, $I_{dc}$, in the system (10) satisfies*

$$d^* = \sup |I_{dc}(t)|, \tag{29}$$

*where $d^*$ is the bound of $I_{dc}$. and*

$$\lim_{t \to \infty} \dot{I}_{dc}(t) = 0. \tag{30}$$

**Remark 7.** *It should be noted that Assumption 3 is always acceptable in DC microgrids [31].*

**Proposition 1.** *Consider the system in (10), if the observer of $I_{dc}$ is designed based on [44] as follows:*

$$\dot{z} = \frac{\ell}{C}(-z + \frac{P_{rec}}{V_{dc}} + \ell V_{dc})$$
$$\hat{I}_{dc} = z - \ell V_{dc}, \tag{31}$$

*where $z$ is the intermediate state, and $\ell > 0$ is the observer gain, then, $\hat{I}_{dc}$ converges to $I_{dc}$ as time tends to infinity.*

*Proof.* Firstly, $e_{I_{dc}} = I_{dc} - \hat{I}_{dc}$ is defined. Then, the time derivative of $e_{I_{dc}}$ is obtained as follows:

$$\dot{e}_{I_{dc}} = \dot{I}_{dc} - \dot{\hat{I}}_{dc}$$
$$\implies = -\frac{\ell}{C}e_{I_{dc}} + \dot{I}_{dc}. \tag{32}$$

If $\ell > 0$, then $e_{I_{dc}}$ will exponentially converge to zero based on (30). $\square$

Consequently, the whole block diagram of the proposed control method is shown in Fig. 3. It should be noted that the observer generates a signal that will be used in the SMC method.

TABLE I
SYSTEM PARAMETERS USED IN SIMULATIONS AND EXPERIMENTS.

| Parameter | Symbol | Value | Unit |
|---|---|---|---|
| Power rating | $S_{rate}$ | 15 | kVA |
| Nominal grid voltage | $V_{sa,rms}$ | 150 | V |
| Nominal grid frequency | $f_s$ | 50 | Hz |
| Filter inductance | $L_s$ | 6 | mH |
| Filter resistance | $R_s$ | 0.6 | Ω |
| Dc-link voltage | $V_{dc}$ | 450 | V |
| Dc-link capacitance | $C$ | 1.1 | mF |
| Switching frequency | $f_{sw}$ | 10 | kHz |
| Sampling frequency | $f_{sa}$ | 10 | kHz |

TABLE II
CONTROLLER GAINS OF THREE CONTROL METHODS. IOL:
INPUT-OUTPUT LINEARIZATION; SMC: SLIDING MODE CONTROL.

| Methods | $K_{P,V_{dc}}$ | $K_{I,V_{dc}}$ | $K_s$ | $\varepsilon$ | $\ell$ |
|---|---|---|---|---|---|
| PI method | 100 | 2500 | - | - | - |
| IOL in (33) | 100 | 2500 | - | - | - |
| SMC in (28) | 1 | 10 | 100 | 0.2 | - |
| Proposed control method in (28)+(31) | 1 | 10 | 100 | 0.5 | 50 |

TABLE III
DC-LINK VOLTAGE PERFORMANCE COMPARISONS OF FOUR CONTROL
METHODS WHEN THE DC LOAD IS CHANGED FROM 460 Ω TO 153 Ω.
CONVERGENCE TIME: DC-LINK VOLTAGE REACHES ±0.1 V.

| Methods | Overshoot | Convergence time |
|---|---|---|
| PI method | 2.27% | 204 ms |
| IOL in (33) | 0.33% | 34 ms |
| SMC in (28) | 0.19% | 3.3 ms |
| Proposed control method in (28)+(31) | 0.21% | 3.3 ms |
| Control implementation has $-30\%$ of $C$ | | |
| IOL in (33) | 0.36% | 43 ms |
| SMC in (28) | 0.20% | 4.2 ms |
| Proposed control method in (28)+(31) | 0.25% | 5.6 ms |
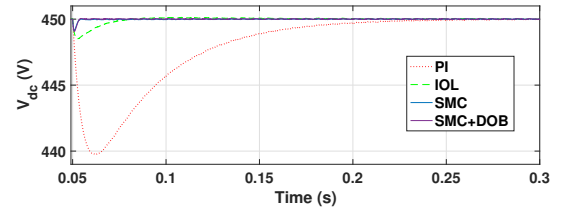


Fig. 4. Dc-link voltage when the dc load is changed from 460 Ω to 153 Ω. at 0.05 s.

## IV. PERFORMANCE VALIDATION

In order to validate the proposed control algorithm, both simulation and experimental setup are done. The parameters of the system used in the simulations and experimental tests are listed in Table I. The performance of the proposed method is compared with those of the SMC using current measurement in (28) and the IOL method given as

$$P_{rec} = I_{dc}V_{dc} + CV_{dc}\left(K_{P,V_{dc}}e_{V_{dc}} + K_{I,V_{dc}}\int e_{V_{dc}}dt\right), \quad (33)$$

which has a better performance compared to the conventional PI and feedforward methods [27]. It should be noted that the inner loop is using the same control strategy and gains, the VM-DPC. The controller gains of all three methods are listed in Table II.

### A. Simulation Results

In the simulation part, all three control algorithms are implemented in MATLAB/Simulink and the electrical system is constructed in PLECS blockset.

The first case is that a dc load (100 Ω) is suddenly connected to the dc-link at 0.05 s. The red-dotted line is the PI method, the solid-blue line is the SMC method with the dc current measurement in (28), the dashed-green line is the IOL method in (33), and the dash-dotted-purple line is the proposed method. As shown in Fig. 4, the PI method has the largest overshoot and slowest convergence time among four methods. From Fig. 5(c), it can be observed that the SMC method with the dc current measurement has the fastest convergence time and smallest overshoot in the dc-link voltage compared to the IOL and the proposed methods. However, the proposed control method only slightly increases the overshoot of dc-link voltage compared with the SMC using the current measurement. In addition, the reactive power is changed from 0 Var to 1 kVar at 0.75 s. All three methods have a small overshoot at the

real power and in the dc voltage. A comparison of overshoot and convergence time of the dc-link voltage is summarized in Table III. Fig. 6 shows that the trajectory with the proposed method reaches its sliding surface in a finite time and remains inside the boundary layer in accordance with Theorem 2. After that, it converges to its equilibrium point smoothly. Finally, we also test a case where there is a parameter mismatch between the control implementation and real system and the capacitance of the dc-link capacitor will be decreased after a certain operation time. In this case, we assume that the capacitance in the control implementation has $-30\%$ of the nominal value. From Fig. 7, we can observe that the performance of the proposed control method is slightly affected by the parameter mismatch, but it is still better than the performance of the IOL method without parameter mismatch. The performance of the IOL method is adversely affected since the IOL method is sensitive to parameter and model accuracies.

We also test the proposed method by considering of unbalanced/distorted grid voltages. Fig. 8 shows the performance of the proposed control method when $v_{s,a}$ has 10% sag, and Fig. 9 shows the performance of the proposed method when the grid voltages have 2% 5th and 1% 7th harmonics, where the total harmonic distortion (THD) is 2.2%. From the results compared with Fig. 5, it can be observed that the system with the proposed method is working well at such operation conditions.

### B. Experimental Results

The effectiveness of the proposed method is validated by using a three-phase 15-kVA voltage source converter with an $L$ filter. Three control algorithms are implemented in the DS1007 dSPACE system, as shown in Fig. 10(a). The ac grid voltages
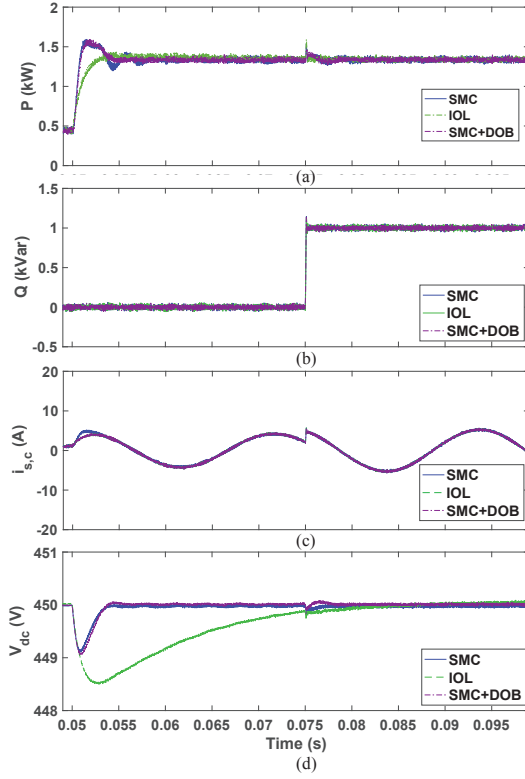
Fig. 5. Simulation results when the dc load is changed from $460\ \Omega$ to $153\ \Omega$. at 0.05 s and the reactive power is changed from 0 Var to 1 kVar at 0.75 s. (a) Real power; (b) reactive power; (c) $i_{s,c}$ line current; (d) dc-link voltage.
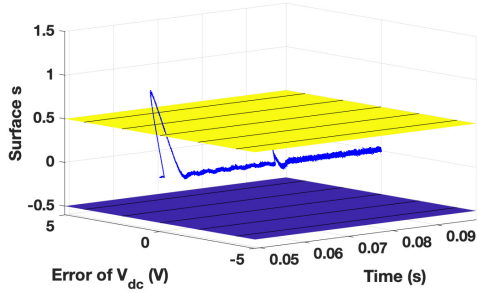


Fig. 6. System trajectory with the proposed control method and sliding surface (25) when the load is connected to the dc-link and the reactive power is changed.
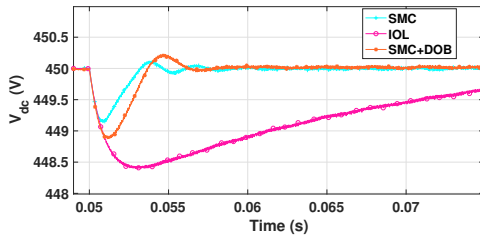


Fig. 7. Dc-link voltage when the capacitance of the dc-link capacitor has $-30\%$ error in the control implementation.
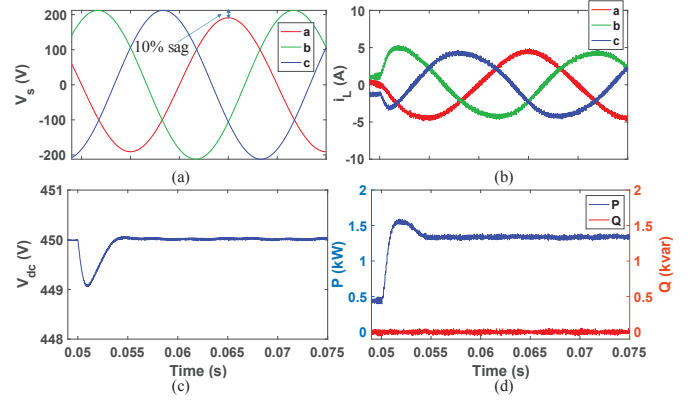


Fig. 8. Simulation results when the dc load is changed from $460\ \Omega$ to $153\ \Omega$ at 0.05 s and $v_{s,a}$ has 10% sag. (a) Grid voltage; (b) $i_{s,c}$ current; (c) dc-link voltage; (b) real and reactive power.
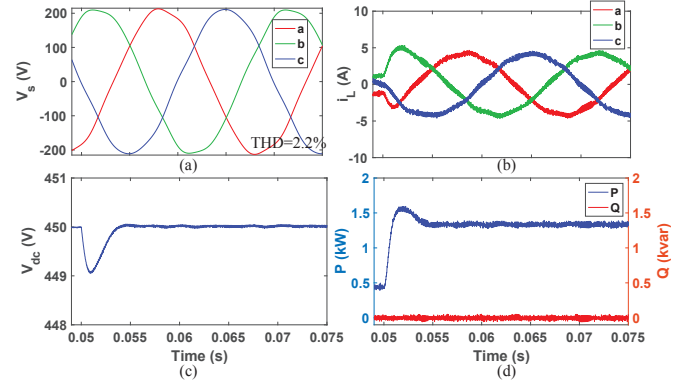


Fig. 9. Simulation results when the dc load is changed from $460\ \Omega$ to $153\ \Omega$ at 0.05 s and the THD of the grid voltage is 2.2%. (a) Grid voltage; (b) $i_{s,c}$ current; (c) dc-link voltage; (b) real and reactive power.

are generated through a grid simulator and measured by using the DS2004 high-speed analog-to-digital board. Moreover, in the dc-link, a resistive load and an inverter with resistive loads are connected, as shown in Fig. 10(b).

In the first case, the dc load is changed from $460\ \Omega$ to $153\ \Omega$, as shown in Fig. 11. It can be observed that the IOL method has the largest overshoot and longest convergence time of the dc-link voltage compared to the two other methods, and a comparison of overshoot and convergence time is summarized in Table IV. The proposed method has a slightly smaller overshoot and larger convergence time of the dc-link voltage than those of the SMC method using the current measurement, since the observer introduces a slight lag. On the other hand, the observer is able to decrease the effect from the unbalanced ac currents caused by the unbalanced parameters on the ac-side, which cause harmonic oscillations on the dc-side, as shown in Fig. 11. Fig. 12 shows the measured performance when the reactive power is changed from 0 Var to 1 kVar. The proposed method and the SMC method with the current measurement have a slightly larger overshoot and longer convergence time. However, the IOL method has larger overshoot and longer convergence time even though the inner loop controller is the same.

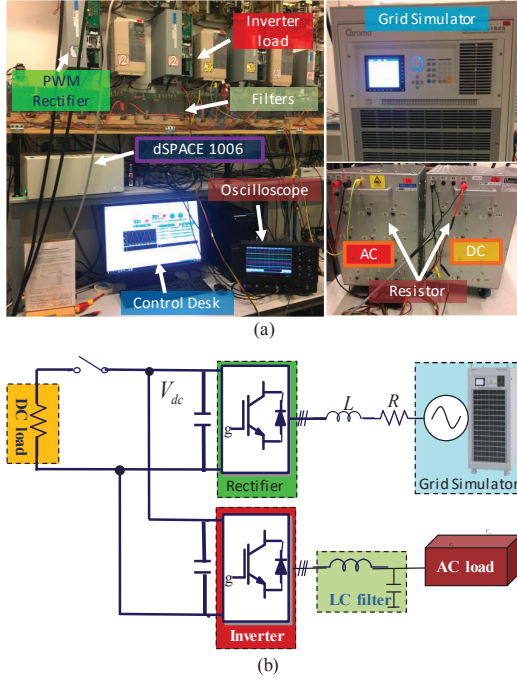The robustness to the parameter uncertainty is also tested,

Fig. 10. Test system for control of rectifier system. (a) Photo of experimental setup, (b) system configuration.
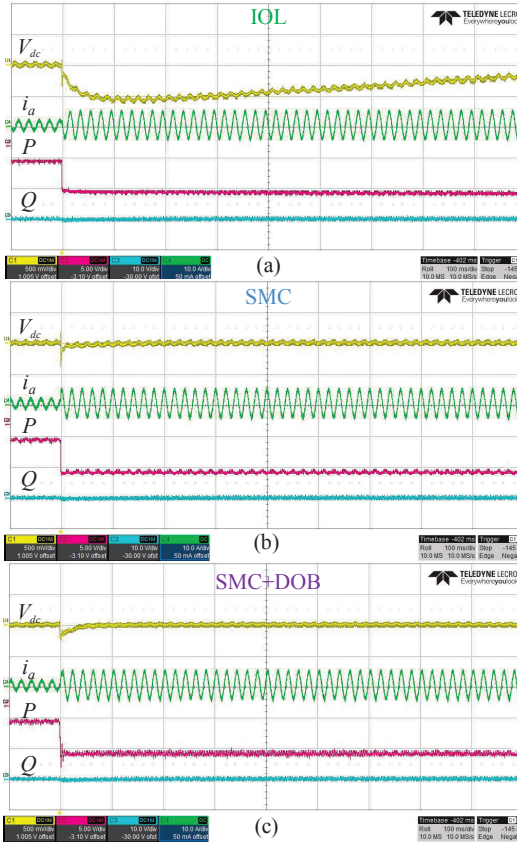


Fig. 11. Measured performance when the dc load is changed from $460\ \Omega$ to $153\ \Omega$. (a) IOL, (b) SMC using measurement, (c) proposed control method. (Yellow line: $V_{dc}$ [5 V/div], green line: $i_{s,a}$ [10 A/div], pink-red line: $P$ [1 kW/div], and sky-blue line: $Q$ [2 kVar/div].)

TABLE IV
MEASURED PERFORMANCE OF DC-LINK VOLTAGE AMONG THREE CONTROL METHODS WHEN THE DC LOAD IS CHANGED FROM 460 Ω TO 153 Ω. CONVERGENCE TIME: DC-LINK VOLTAGE REACHES ±0.5 V.

| Methods | Overshoot | Convergence time |
|---|---|---|
| IOL in (33) | 1.33% | > 900 ms |
| SMC in (28) | 0.89% | 40 ms |
| Proposed control method in (28)+(31) | 0.44% | 60 ms |
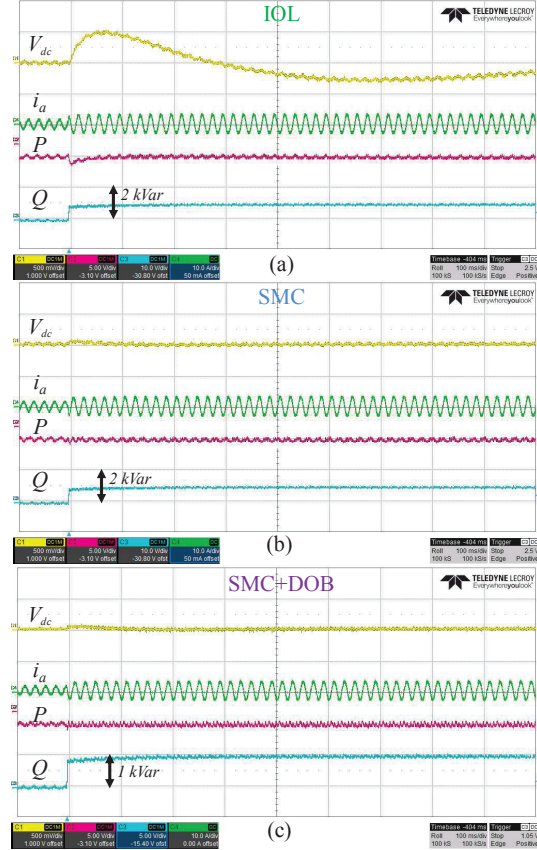


Fig. 12. Measured performance when the reactive power is changed from $0$ Var to $1$ kVar. (a) IOL, (b) SMC, (c) proposed control method. (Yellow line: $V_{dc}$ [5 V/div], green line: $i_{s,a}$ [10 A/div], pink-red line: $P$ [1 kW/div], and sky-blue line: $Q$ [2 kVar/div].)

as shown in Fig. 13, where the capacitance of the dc capacitor has $-30\%$ error in the control implementation. It can be seen that the IOL method is the most sensitive to the parameter uncertainties compared to the other two methods. The proposed method has a slightly larger overshoot due to the parameter uncertainty. Lastly, a CPL (e.g., an inverter) is connected into the dc microgrid. From Fig. 14, it can be seen that the proposed method is regulating the dc-link voltage well even when the CPL is suddenly connected into the dc microgrid.

## V. CONCLUSIONS

A three-phase PWM rectifier was controlled by the proposed control strategy, which has a dc-link current observer based SMC in the outer loop and a voltage modulated-DPC in the inner loop. The SMC was applied to generate the real power

Fig. 13. Measured performance when the capacitance of the dc capacitor has $-30\%$ error in the control implementation. (a) IOL, (b) SMC using measurement, (c) proposed control method. (Yellow line: $V_{dc}$ [5 V/div], green line: $i_{s,a}$ [10 A/div], pink-red line: $P$ [1 kW/div], and sky-blue line: $Q$ [2 kVar/div].)
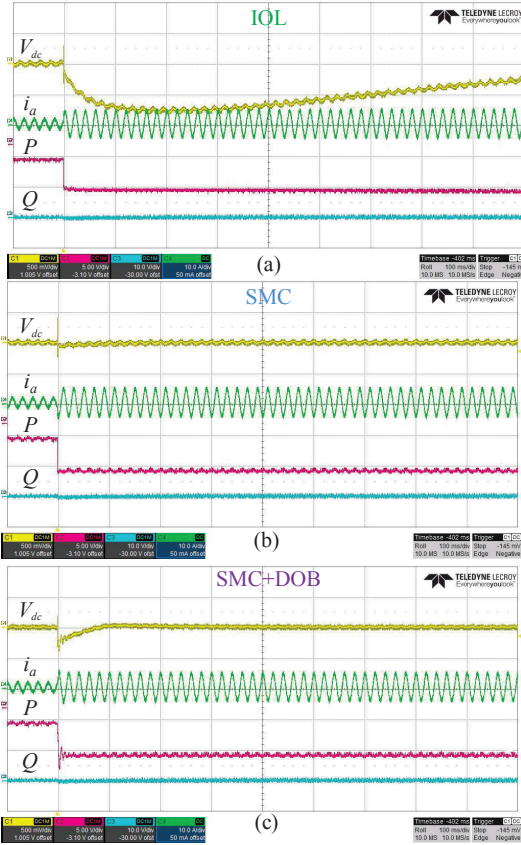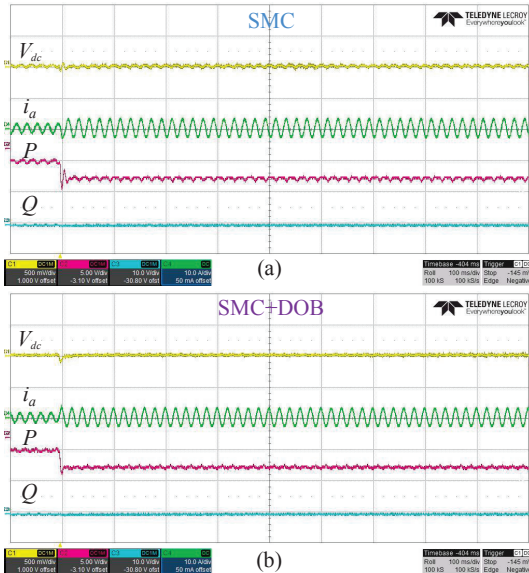


Fig. 14. Measured performance when a CPL is connected. (a) SMC using measurement, (b) proposed control method. (Yellow line: $V_{dc}$ [5 V/div], green line: $i_{s,a}$ [10 A/div], pink-red line: $P$ [1 kW/div], and sky-blue line: $Q$ [2 kVar/div].)

reference in the inner loop in order to make sure the dc-link voltage to be within a certain level in the dc microgrids even there exist CPLs. Furthermore, an observer for the dc-link current was designed in order to remove the need for a current sensor. Both simulation and experimental results show that the proposed method effectively reduces the overshoot of the dc-link voltage and is robust to parameter mismatch of the capacitance value in the dc-link.

## REFERENCES

[1] J. Liu, X. Lu, and J. Wang, "Resilience analysis of DC microgrids under denial of service threats," *IEEE Trans. Power Syst.*, vol. 34, no. 4, pp. 3199–3208, July 2019.

[2] F. Blaabjerg, M. Liserre, and K. Ma, "Power electronics converters for wind turbine systems," *IEEE Trans. Ind. Appl.*, vol. 48, no. 2, pp. 708–719, 2012.

[3] B. Wei, Y. Gui, A. Marzabal, Trujillo, J. M. Guerrero, and J. C. Vasquez, "Distributed average secondary control for modular UPS systems based microgrids," *IEEE Trans. Power Electron.*, vol. 34, no. 7, pp. 6922–6936, July 2019.

[4] F. Blaabjerg, R. Teodorescu, M. Liserre, and A. V. Timbus, "Overview of control and grid synchronization for distributed power generation systems," *IEEE Trans. Ind. Electron.*, vol. 53, no. 5, pp. 1398–1409, 2006.

[5] M. Kazmierkowski and L. Malesani, "Current control techniques for three-phase voltage-source PWM converters: a survey," *IEEE Trans. Ind. Electron.*, vol. 45, no. 5, pp. 691–703, Oct 1998.

[6] T. Noguchi, H. Tomiki, S. Kondo, and I. Takahashi, "Direct power control of PWM converter without power-source voltage sensors," *IEEE Trans. Ind. Appl.*, vol. 34, no. 3, pp. 473–479, 1998.

[7] M. Malinowski, M. Jasiński, and M. P. Kazmierkowski, "Simple direct power control of three-phase PWM rectifier using space-vector modulation (DPC-SVM)," *IEEE Trans. Ind. Electron.*, vol. 51, no. 2, pp. 447–454, 2004.

[8] A. Bouafia, J. Gaubert, and F. Krim, "Predictive direct power control of three-phase pulsewidth modulation (PWM) rectifier using space-vector modulation (SVM)," *IEEE Trans. Power Electron.*, vol. 25, no. 1, pp. 228–236, Jan 2010.

[9] J. Hu, L. Shang, Y. He, and Z. Zhu, "Direct active and reactive power regulation of grid-connected DC/AC converters using sliding mode control approach," *IEEE Trans. Power Electron.*, vol. 26, no. 1, pp. 210–222, 2011.

[10] Y. Gui, G. H. Lee, C. Kim, and C. C. Chung, "Direct power control of grid connected voltage source inverters using port-controlled Hamiltonian system," *Int. J. Control Autom. Syst.*, vol. 15, no. 5, pp. 2053–2062, 2017.

[11] S. Vazquez, J. Rodriguez, M. Rivera, L. G. Franquelo, and M. Norambuena, "Model predictive control for power converters and drives: Advances and trends," *IEEE Trans. Ind. Electron.*, vol. 64, no. 2, pp. 935–947, 2017.

[12] Y. Gui, X. Wang, F. Blaabjerg, and D. Pan, "Control of grid-connected voltage-source converters: The relationship between direct-power control and vector-current control," *IEEE Ind. Electron. Mag.*, vol. 13, no. 2, pp. 31–40, June 2019.

[13] Y. Gui, C. Kim, C. C. Chung, J. M. Guerrero, Y. Guan, and J. C. Vasquez, "Improved direct power control for grid-connected voltage source converters," *IEEE Trans. Ind. Electron.*, vol. 65, no. 10, pp. 8041–8051, Oct 2018.

[14] R.-J. Wai and Y. Yang, "Design of backstepping direct power control for three-phase PWM rectifier," *IEEE Trans. Ind. Appl.*, vol. 55, no. 3, pp. 3160–3173, 2019.

[15] W. Gil-González, O. D. Montoya, and A. Garces, "Direct power control for VSC-HVDC systems: An application of the global tracking passivity-based PI approach," *Int. J. Electr. Power Energy Syst.*, vol. 110, pp. 588–597, 2019.

[16] S. Gao, H. Zhao, Y. Gui, Z. Zhang, and Q. Wu, "A voltage modulated direct power control of the doubly fed induction generator," in *Proc, IEEE Power Energy Soc. General Meeting*, 2019, pp. 1–5.

[17] Y. Gui, B. Wei, M. Li, J. M. Guerrero, and J. C. Vasquez, "Passivity-based coordinated control for islanded AC microgrid," *Appl. Energy*, vol. 229, pp. 551–561, 2018.

[18] Y. Gui, X. Wang, H. Wu, and F. Blaabjerg, "Voltage modulated direct power control for a weak grid-connected voltage source inverters," *IEEE Trans. Power Electron.*, vol. 34, no. 11, pp. 11 383–11 395, Nov 2019.

[19] Y. Gui, X. Wang, and F. Blaabjerg, "Vector current control derived from direct power control for grid-connected inverters," *IEEE Trans. Power Electron.*, vol. 34, no. 9, pp. 9224–9235, Sep. 2019.

[20] Y. Gui, Q. Xu, F. Blaabjerg, and H. Gong, "Sliding mode control with grid voltage modulated DPC for voltage source inverters under distorted grid voltage," *CPSS Trans. Power Electron. Appl.*, vol. 4, no. 3, pp. 244–254, Sep. 2019.

[21] A. Timbus, M. Liserre, R. Teodorescu, P. Rodriguez, and F. Blaabjerg, "Evaluation of current controllers for distributed power generation systems," *IEEE Trans. Power Electron.*, vol. 24, no. 3, pp. 654–664, March 2009.

[22] L. Malesani, L. Rossetto, P. Tenti, and P. Tomasin, "AC/DC/AC PWM converter with reduced energy storage in the DC link," *IEEE Trans. Ind. Appl.*, vol. 31, no. 2, pp. 287–292, 1995.

[23] M.-T. Tsai and W.-I. Tsai, "Analysis and design of three-phase AC-to-DC converters with high power factor and near-optimum feedforward," *IEEE Trans. Ind. Electron.*, vol. 46, no. 3, pp. 535–543, 1999.

[24] A. Yazdani and R. Iravani, *Voltage-sourced converters in power systems: modeling, control, and applications*. John Wiley & Sons, 2010.

[25] M. Davari and Y. A.-R. I. Mohamed, "Dynamics and robust control of a grid-connected VSC in multiterminal DC grids considering the instantaneous power of DC-and AC-side filters and DC grid uncertainty," *IEEE Trans. Power Electron.*, vol. 31, no. 3, pp. 1942–1958, 2016.

[26] M. Merai, M. W. Naouar, and I. Slama-Belkhodja, "An improved DC-link voltage control strategy for grid connected converters," *IEEE Trans. Power Electron.*, vol. 33, no. 4, pp. 3575–3582, 2017.

[27] Y. Gui, M. Li, J. Lu, S. Golestan, J. M. Guerrero, and J. C. Vasquez, "A voltage modulated DPC approach for three-phase PWM rectifier," *IEEE Trans. Ind. Electron.*, vol. 65, no. 10, pp. 7612–7619, Oct 2018.

[28] A. Rodríguez-Cabero, M. Prodanovic, and J. Roldán-Pérez, "Full-state feedback control of back-to-back converters based on differential and common power concepts," *IEEE Trans. Ind. Electron.*, vol. 66, no. 11, pp. 9045–9055, 2019.

[29] J. Liu, S. Vazquez, L. Wu, A. Marquez, H. Gao, and L. G. Franquelo, "Extended state observer-based sliding-mode control for three-phase power converters," *IEEE Trans. Ind. Electron.*, vol. 64, no. 1, pp. 22–31, 2017.

[30] R. Ghosh and G. Narayanan, "Generalized feedforward control of single-phase PWM rectifiers using disturbance observers," *IEEE Trans. Ind. Electron.*, vol. 54, no. 2, pp. 984–993, 2007.

[31] C. Wang, X. Li, L. Guo, and Y. W. Li, "A nonlinear-disturbance-observer-based DC-bus voltage control for a hybrid AC/DC microgrid," *IEEE Trans. Power Electron.*, vol. 29, no. 11, pp. 6162–6177, 2014.

[32] Z. Pan, X. Wang, T. T. G. Hoang, Z. Wang, and L. Tian, "DC-link voltage disturbance rejection strategy of PWM rectifiers based on reduced-order LESO," *IEEE Access*, vol. 7, pp. 103 693–103 705, 2019.

[33] X. Wang and F. Blaabjerg, "Harmonic stability in power electronic-based power systems: Concept, modeling, and analysis," *IEEE Trans/ Smart Grid*, vol. 10, no. 3, pp. 2858–2870, May 2019.

[34] A. Levant, "Sliding order and sliding accuracy in sliding mode control," *Int. J. Control*, vol. 58, no. 6, pp. 1247–1263, 1993.

[35] Y. Gui, J. Bendtsen, and J. Stoustrup, "Sliding mode control with grid voltage modulated direct power control for three-phase AC-DC converter," in *38th Chinese Control Conference*, 2019, pp. 7436–7441.

[36] H. Gholami-Khesht, M. Monfared, and S. Golestan, "Low computational burden grid voltage estimation for grid connected voltage source converter-based power applications," *IET Power Electron.*, vol. 8, no. 5, pp. 656–664, 2015.

[37] C. A. Busada, S. Gomez Jorge, and J. A. Solsona, "Full-state feedback equivalent controller for active damping in LCL-filtered grid-connected inverters using a reduced number of sensors," *IEEE Trans. Ind. Electron.*, vol. 62, no. 10, pp. 5993–6002, Oct 2015.

[38] H. Yang, Y. Zhang, J. Liang, J. Gao, P. D. Walker, and N. Zhang, "Sliding-mode observer based voltage-sensorless model predictive power control of PWM rectifier under unbalanced grid conditions," *IEEE Trans. Ind. Electron.*, vol. 65, no. 7, pp. 5550–5560, July 2018.

[39] R. A. Fantino, C. A. Busada, and J. A. Solsona, "Observer-based grid-voltage sensorless synchronization and control of a VSI-LCL tied to an unbalanced grid," *IEEE Trans. Ind. Electron.*, vol. 66, no. 7, pp. 4972–4981, July 2019.

[40] A. Rahoui, A. Bechouche, H. Seddiki, and D. O. Abdeslam, "Grid voltages estimation for three-phase PWM rectifiers control without AC voltage sensors," *IEEE Trans. Power Electron.*, vol. 33, no. 1, pp. 859–875, Jan 2018.

[41] P. Cortes, J. Rodriguez, P. Antoniewicz, and M. Kazmierkowski, "Direct power control of an AFE using predictive control," *IEEE Trans. Power Electron.*, vol. 23, no. 5, pp. 2516–2523, 2008.

[42] A. P. N. Tahim, D. J. Pagano, E. Lenz, and V. Stramosk, "Modeling and stability analysis of islanded DC microgrids under droop control," *IEEE Transactions on Power Electronics*, vol. 30, no. 8, pp. 4597–4607, Aug 2015.

[43] Y. Gui, C. Kim, and C. C. Chung, "Grid voltage modulated direct power control for grid connected voltage source inverters," in *Amer. Control Conf.*, 2017, pp. 2078–2084.

[44] W.-H. Chen, J. Yang, L. Guo, and S. Li, "Disturbance-observer-based control and related methods—An overview," *IEEE Trans. Ind. Electron.*, vol. 63, no. 2, pp. 1083–1095, 2016.

**Yonghao Gui** (S'11-M'17) received the B.S. degree in automation from Northeastern University, Shenyang, China, in 2009, and the M.S. and Ph.D. degrees in electrical engineering from Hanyang University, Seoul, South Korea, in 2012 and 2017, respectively.

From Feb. 2017 to Nov. 2018, he worked with the Department of Energy Technology, Aalborg University, Aalborg, Denmark, as a Postdoctoral Researcher. Since Dec. 2018, he has been working with the Automation & Control Section, Department of Electronic Systems, Aalborg University, Aalborg, Denmark, where he is currently an Assistant Professor. His research interests include Control of Power Electronics in Power Systems, Energy Internet, and Smart Grids.

Dr. Gui has served as an Associate Editor for the IEEE ACCESS and the International Journal of Control, Automation and Systems (IJCAS). He was a recipient of the IEEE Power & Energy Society General Meeting Best Conference Paper Award in 2019 the IJCAS Academic Activity Award 2019.

**Frede Blaabjerg** (S'86-M'88-SM'97-F'03) was with ABB-Scandia, Randers, Denmark, from 1987 to 1988. From 1988 to 1992, he got the PhD degree in Electrical Engineering at Aalborg University in 1995. He became an Assistant Professor in 1992, an Associate Professor in 1996, and a Full Professor of power electronics and drives in 1998. From 2017 he became a Villum Investigator. He is honoris causa at University Politehnica Timisoara (UPT), Romania and Tallinn Technical University (TTU) in Estonia.

His current research interests include power electronics and its applications such as in wind turbines, PV systems, reliability, harmonics and adjustable speed drives. He has published more than 600 journal papers in the fields of power electronics and its applications. He is the co-author of four monographs and editor of ten books in power electronics and its applications.

He has received 32 IEEE Prize Paper Awards, the IEEE PELS Distinguished Service Award in 2009, the EPE-PEMC Council Award in 2010, the IEEE William E. Newell Power Electronics Award 2014, the Villum Kann Rasmussen Research Award 2014, the Global Energy Prize in 2019 and the 2020 IEEE Edison Medal. He was the Editor-in-Chief of the IEEE TRANSACTIONS ON POWER ELECTRONICS from 2006 to 2012. He has been Distinguished Lecturer for the IEEE Power Electronics Society from 2005 to 2007 and for the IEEE Industry Applications Society from 2010 to 2011 as well as 2017 to 2018. In 2019-2020 he serves a President of IEEE Power Electronics Society. He is Vice-President of the Danish Academy of Technical Sciences too. He is nominated in 2014-2019 by Thomson Reuters to be between the most 250 cited researchers in Engineering in the world.

**Xiongfei Wang** (S'10-M'13-SM'17) received the B.S. degree from Yanshan University, Qinhuang-dao, China, in 2006, the M.S. degree from Harbin Institute of Technology, Harbin, China, in 2008, both in electrical engineering, and the Ph.D. degree in energy technology from Aalborg University, Aalborg, Denmark, in 2013.

Since 2009, he has been with the Department of Energy Technology, Aalborg University, where he became an Assistant Professor in 2014, an Associate Professor in 2016, a Professor and Research Program Leader for Electronic Power Grid (eGrid) in 2018, and the Director of Aalborg University-Huawei Energy Innovation Center in 2020. His current research interests include modeling and control of grid-interactive power converters, stability and power quality of converter-based power systems, active and passive filters.

Dr. Wang was selected into Aalborg University Strategic Talent Management Program in 2016. He has received six IEEE Prize Paper Awards, the 2016 Outstanding Reviewer Award of IEEE TRANSACTIONS ON POWER ELECTRONICS, the 2018 IEEE PELS Richard M. Bass Outstanding Young Power Electronics Engineer Award, the 2019 IEEE PELS Sustainable Energy Systems Technical Achievement Award, and the 2019 Highly Cited Researcher by Clarivate Analytics (former Thomson Reuters). He serves as a Member at Large for Administrative Committee of IEEE Power Electronics Society in 2020-2022, and as an Associate Editor for the IEEE TRANSACTIONS ON POWER ELECTRONICS, the IEEE TRANSACTIONS ON INDUSTRY APPLICATIONS, and the IEEE JOURNAL OF EMERGING AND SELECTED TOPICS IN POWER ELECTRONICS.

**Jan D. Bendtsen** (M'11) was born in Denmark in 1972. He received the M.Sc.E.E. degree in 1996 and the Ph.D. degree from the Department of Control Engineering, Aalborg University, Aalborg, Denmark in 1999, respectively.

Since 2003, he has been an Associate Professor with the Department of Electronic Systems, Aalborg University. In 2005, he was a Visiting Researcher with the Australian National University, Australia. Since 2006, he has been on the organizing committee of several international conferences. From 2012 to 2013, he was a Visiting Researcher with the University of California at San Diego, USA. His current research interests include adaptive control of nonlinear systems, closed-loop system identification, control of distribution systems, and infinite-dimensional systems.

Dr. Bendtsen was a corecipient of the Best Technical Paper Award at the AIAA Guidance, Navigation, and Control Conference in 2009.

**Dongsheng Yang** (S'13-M'17-SM'19) received the B.S., M.S., and Ph.D. degrees in electrical engineering from Nanjing University of Aeronautics and Astronautics, Nanjing, China, in 2008, 2011, and 2016, respectively.

In 2016, he joined Aalborg University, Aalborg, Denmark as a postdoc researcher, where he became the Assistant Professor in the Department of Energy Technology in 2018. Since 2019, Dr. Yang has worked within the Electrical Energy Systems group at Eindhoven University of Technology (TU/e) as the Assistant Professor. His main research interests include modeling, analysis, and control of grid-interactive converters, harmonic and resonance mitigation of large-scale power electronics based power system, impedance measurement technique for real-field harmonic instability assessment, innovative hardware of power-electronics-based infrastructure for future power grids.

**Jakob Stoustrup** (M'87-SM'99) has received an M.Sc. degree (EE, 1987) and a Ph.D. degree (Applied Mathematics, 1991), both from the Technical University of Denmark. From 1991-1996, Dr. Stoustrup held several positions at the Department of Mathematics, Technical University of Denmark. From 2006-2013 he acted as Head of Research for Department of Electronic Systems, Aalborg University. From 2014-2016, Stoustrup was Chief Scientist at Pacific Northwest National Laboratory, USA, leading the Control of Complex Systems Initiative. From 1997-2013 and since 2016, Stoustrup has acted as Professor at Automation & Control, Aalborg University, Denmark. In 2017 Stoustrup was appointed as Vice Dean at the Technical Faculty of IT and Design, Aalborg University.

Dr. Stoustrup has acted as Associate Editor and Editorial Board Member of several international journals. Served as General Chair, Program Chair, and IPC member for several international conferences. Member of the IEEE CSS Board of Governors. Past Chairman of IEEE CSS/RAS Joint Chapter. Chair for IEEE CSS Technical Committee on Smart Grids. Chair for IFAC Technical Committee SAFEPROCESS, and Member of IFAC Technical Board. Received the Statoil Prize, the Dannin Award for Scientific Research and several conference paper awards. He has received the Chivalric Order of the Dannebrog for his research contributions. Member of the European Research Council as well as the Danish, Norwegian and Swedish Research Councils. He is a member of The Danish Academy of Technical Sciences, where he has acted as Board Member.

Stoustrup's main contributions have been to robust control theory and to the theory of fault tolerant control systems. With co-workers, he has proposed a novel Plug-and-Play Control framework. Published approx. 300 peer-reviewed scientific papers. Apart from the theoretical work, he has been involved in applications in cooperation with 100+ industrial companies, including acting as CEO for two technological startup companies.